

JGR Solid Earth

RESEARCH ARTICLE

10.1029/2019JB018727

Key Points:

- The crustal thickness varies significantly across and along major tectonic units
- A ~12–15 km west-east Moho offset is observed within a narrow zone in the central Appalachians and is interpreted to represent a sharp Laurentia-Gondwana boundary
- The Grenville-aged crust differs between the northern and southern parts with a dipping intracrustal layer in the central Grenville Province

Supporting Information:

- Supporting Information S1
- Table S1
- Movie S1

Correspondence to:

C. Li,
conli@geo.umass.edu

Citation:

Li, C., Gao, H., & Williams, M. L. (2020). Seismic characteristics of the eastern North American crust with Ps converted waves: Terrane accretion and modification of continental crust.

Journal of Geophysical Research: Solid Earth, 125, e2019JB018727. <https://doi.org/10.1029/2019JB018727>

Received 19 SEP 2019

Accepted 14 APR 2020

Accepted article online 20 APR 2020

Seismic Characteristics of the Eastern North American Crust With Ps Converted Waves: Terrane Accretion and Modification of Continental Crust

Cong Li¹ , Haiying Gao¹ , and Michael L. Williams¹ 

¹Department of Geosciences, University of Massachusetts Amherst, Amherst, MA, USA

Abstract The impact of past tectonic events on the formation and modification of continental lithosphere remains as an open question of fundamental importance. Eastern North America provides a complete record of supercontinent assembly and breakup over the past 1.3 Ga, serving as a natural laboratory for our understanding of continental crust and mantle lithosphere and for integrating geologic and geophysical observations. In this study, we used teleseismic Ps receiver functions to image the detailed distribution of crustal thickness beneath eastern North America. The radial-component receiver functions were calculated from seismic waveforms recorded by a total of 659 broadband stations during 2010–2017, yielding a high-resolution image of Moho depth distribution. **The depths of the Moho and intracrustal layers vary within and across the major tectonic units.** Specifically, there are distinct differences in crustal thickness between the northern and southern Grenville Province. A dipping intracrustal feature can be seen within the central Grenville Province, with the depth increasing eastward from 5 to 27 km. The Moho depth decreases southeastward across the Grenville-Appalachian boundary, with a sharp Moho offset of up to 12–15 km in the central segment and a more gradual variation to the north and south. The thickness difference between the southern and northern Grenville-aged crusts suggests different tectonic and/or exhumation histories during and after the Grenville Orogeny. The low-angle eastward dipping crustal feature is interpreted to be a Grenville-aged collisional structure. Differences in the steepness of the Moho offset along the strike of Appalachians probably reflect variation of the steepness of the subsurface boundary between Laurentia and accreted terranes with different intensities of postorogenic modification. The observed spatial relation between the geologically defined tectonic boundaries and crustal thickness variations provides new constraints on the depth extent of the tectonic units within the crust.

1. Introduction

The Wilson tectonic cycle is one of the most fundamental concepts in the plate tectonic paradigm, central in most models for the growth and modification of continental crust on Earth. However, questions remain concerning the impact of past tectonic events on the composition and growth history of continental crust and mantle lithosphere. Simple but first-order questions include the following: **Which geologically defined tectonic boundaries can be correlated with subsurface gradients or boundaries in three-dimensional seismic models, and what constraints can seismic data place on the timing and history of these boundaries?** Eastern North America experienced at least two complete Wilson cycles over the last 1.3 Ga from assembly of the supercontinent Rodinia to the formation of the modern Atlantic Ocean (e.g., Hatcher, 2010; Thomas, 2006). Thus, eastern North America provides an excellent tectonic setting to advance our understanding of continental accretion and lithospheric evolution through geologic time as well as the interpretation of deep crustal geophysical data in general.

The deployment of the EarthScope Transportable Array (IRIS Transportable Array, 2003) and its retaining subset (UC San Diego, 2013), together with many other seismic networks, has significantly increased the spatial density of broadband observations in eastern North America and, thus, provide a new opportunity to constrain crustal thickness variations and the extent of crustal discontinuities at a resolution on the order of tens of kilometers. In this contribution, we report new receiver function (RF) results, which highlight variations in crustal characteristics within the major tectonic units and across the major tectonic boundaries. Comparison of our receiver function results with gravity data and geological observations allows us to explore the linkage of major geologically defined tectonic units with the geometry of seismically defined

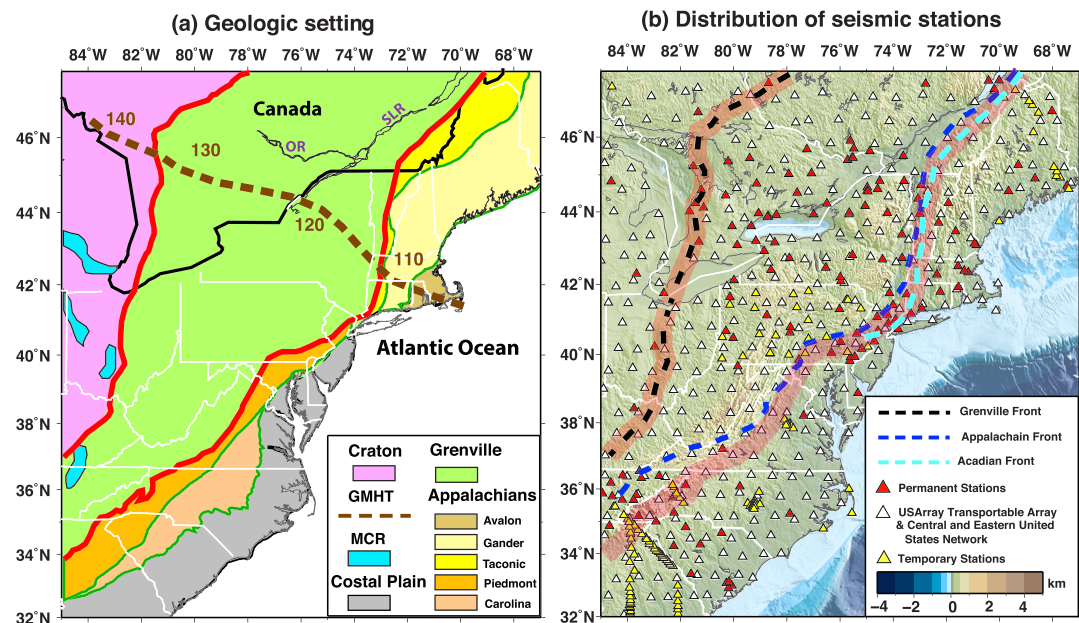


Figure 1. (a) Geological map showing the major tectonic units in eastern North America, modified after the lithotectonic map of the Appalachian orogen by Hibbard et al. (2006) and the United States Geological Survey basement domain map (<http://mrdata.usgs.gov/ds-898/>). The two thick red lines mark the inferred North American craton-Grenville boundary and the Grenville-Appalachian boundary. The dark green lines mark the boundaries between the tectonic subprovinces of Inner Piedmont-Carolina-coastal plain in the southern Appalachian region and Taconic Belt-Gander-Avalon in the northern Appalachian region. The cyan patches denote the inferred eastern arm of the Midcontinent Rift (MCR). The brown dashed line indicates the proposed Great Meteor hot spot track (GMHT), marked with time in Ma. (b) Distribution of the broadband seismic stations used in the calculation of receiver functions. The red triangles represent the permanent stations, the white triangles for the EarthScope U.S. Transportable Array and the central and eastern United States network, and the yellow triangles for the flexible arrays. The black, blue, and cyan dashed lines mark the Grenville deformation front, the Appalachian deformation front, and the Acadian deformation front, respectively. The red shadow zones mark the inferred major tectonic boundaries as shown by the red lines in (a). The background color is the bathymetry/topography.

crustal discontinuities, and ultimately to investigate the formation and modification of the crust from the North American craton through the Grenville Province eastward to the Appalachian accreted region.

2. Tectonic setting and the previous studies

Our study region involves three major tectonic units (Figure 1a), including the North American craton (~3.8–1.3 Ga), the Grenville Province (~1.3–0.98 Ga), and the Appalachian orogenic region (~495–280 Ma) (David et al., 2009; Hatcher, 2010; McLelland et al., 2010, 2013). The North American craton was formed by the amalgamation of several cratonic blocks, including the Archean Superior Craton, the Paleoproterozoic Penokean Province, and the Mesoproterozoic Granite-Rhyolite Province (Card, 1990; McLelland et al., 2010, 2013; Percival et al., 2004; Whitmeyer & Karlstrom, 2007). The Grenville Province involved a series of collisional and extensional events that ultimately resulted in the assembly of the supercontinent Rodinia (Hynes & Rivers, 2010; Rivers, 1997). The Grenville-aged crust experienced different degrees of extensional collapse and erosion after amalgamation (Jamieson et al., 2010; McLelland et al., 2010, 2013). The breakup of Rodinia at ~750 Ma (Hatcher, 2010) led to rifting along the eastern margin of the Grenville Province (Rimando & Benn, 2005).

The Appalachian orogen was formed during the assembly of the supercontinent Pangea from approximately 495 to 280 Ma and involved a sequence of terrane accretion events and the ultimate collision of Laurentia with Gondwana (Hatcher, 2010; van Staal et al., 2009). In the northern Appalachian region, three major exotic terranes have been recognized (Figure 1): from oldest (inboard) to youngest (outboard), the Taconic belt (and possible Moretown terrane), the Gander terrane, and the Avalon terrane (Hatcher, 2010; Karabinos

et al., 2017; van Staal et al., 2009). In the southern Appalachians, two major terranes have been recognized, including the Inner Piedmont terrane and the large exotic Carolina Superterrane (Thomas, 2006). After assembly, several stages of Mesozoic rifting and exhumation ultimately resulted in the modern continental margin (Hatcher, 2010; Thomas, 2006).

Three first-order deformation fronts, the Grenville Front, the Appalachian Front, and the Acadian Front, can be recognized in parts of eastern North America (Figure 1b). The Grenville Front follows the inferred tectonic boundary between the North American craton and the Grenville Province (Figure 1b). This front has been interpreted as a contractional fault system, dating from the Grenville orogeny. It separates the low metamorphic-grade North American craton from the high-grade outcrops in the Canadian Grenville Province (McLelland et al., 2010). The Grenville Front has been traditionally assumed to extend southward into Ohio and Kentucky in the United States (e.g., Stein, Stein, Elling, Keller, & Kley, 2018), where it is not exposed at the surface. The Appalachian Front is a structurally defined boundary between rocks deformed or transported westward during Appalachian orogenesis and flat-lying Paleozoic rocks and underlying Grenville-aged rocks to the west (Mount, 2014). Grenville-aged rocks have been interpreted beneath Paleozoic rocks to the east of the Appalachian Front in the northern and southern Appalachians, suggesting the subsurface extension of the Grenville terrane under accreted Appalachian elements (e.g., Cook & Vasudevan, 2006; Figure 1b). The Acadian Front is the northern and central Appalachian boundary between rocks (and structures) deformed or reactivated during the Devonian Acadian orogeny and rocks deformed by earlier Paleozoic or Precambrian events (Bradley et al., 2000; Robinson et al., 1998). Acadian orogenesis has not been widely recognized in the southern Appalachians (Hibbard & Karabinos, 2013).

Previous studies have demonstrated that the continental crust beneath eastern North America varies within and across the major tectonic units in terms of age, thickness, and seismic velocity. For example, geochronology and lead isotope studies showed that the Grenville-aged crust is on average younger in the United States than in Canada (e.g., Hynes & Rivers, 2010; Loewy et al., 2003). The U.S. Grenville Province is characterized by a thicker crust and is seismically faster above and beneath the Moho in comparison with the Appalachians and the Canadian Grenville Province (e.g., Schmandt et al., 2015; Shen & Ritzwoller, 2016). Receiver function analysis has revealed a low-angle southeastward dipping intracrustal feature across the central Grenville Province (Long et al., 2019) and beneath the southern Appalachians in Georgia and South Carolina (Hopper et al., 2017; Parker et al., 2015). In contrast, no such intracrustal layer was seen in the Appalachian region of New England (Li et al., 2018). Moho depth changes gradually beneath northern New England (Li et al., 2018) and the southern Appalachian orogen in Georgia (Hopper et al., 2017; Parker et al., 2015). In contrast, a sharp Moho step was imaged in southern New England, New Jersey, and northern Virginia (Li et al., 2018; Soto-Cordero et al., 2018). Although significant variations in crustal features were detected, none of those previous studies provide systematic constraints on the crustal structure for the entire eastern North American region.

3. Methodology

3.1. Data

We collected data from a total of 659 broadband seismic stations, including 167 stations from 12 long-running seismic networks (CN, Geological Survey of Canada, 1989; CO, Colorado Geological Survey, 2016; ET, University of Memphis, CERI, 1982; IM; IU, Albuquerque Seismological Laboratory /USGS, 1988; KY, Kentucky Geological Survey/University of Kentucky, 1982; LD, Lamont Doherty Earth Observatory, Columbia University, 1970; N4, UC San Diego, 2013; NE, Albuquerque Seismological Laboratory /USGS, 1994; PE, Penn State University, 2004; PO, Geological Survey of Canada, 2000; WU, University of Western Ontario, 1991), 380 stations from the EarthScope Transportable Array (IRIS Transportable Array, 2003), and 112 temporary stations from 7 dense arrays (X8, Menke et al., 2012; XQ, Wagner, 2012; XY, Penn State University, 2013; YC, Meltzer, 2011; YO, Gaherty et al., 2014; Z4, Wagner, 2009; Z9, Fischer et al., 2010; Figure 1b; see a detailed network description in the supporting information). The well-distributed coverage of the stations across our study region makes it feasible to study the high-resolution variations in crustal thickness beneath eastern North America. Three-component seismograms were requested from the Data Management center of the Incorporated Research Institutions for Seismology (IRIS) for 4,079 earthquakes that occurred between 2010 and 2017. The earthquakes were

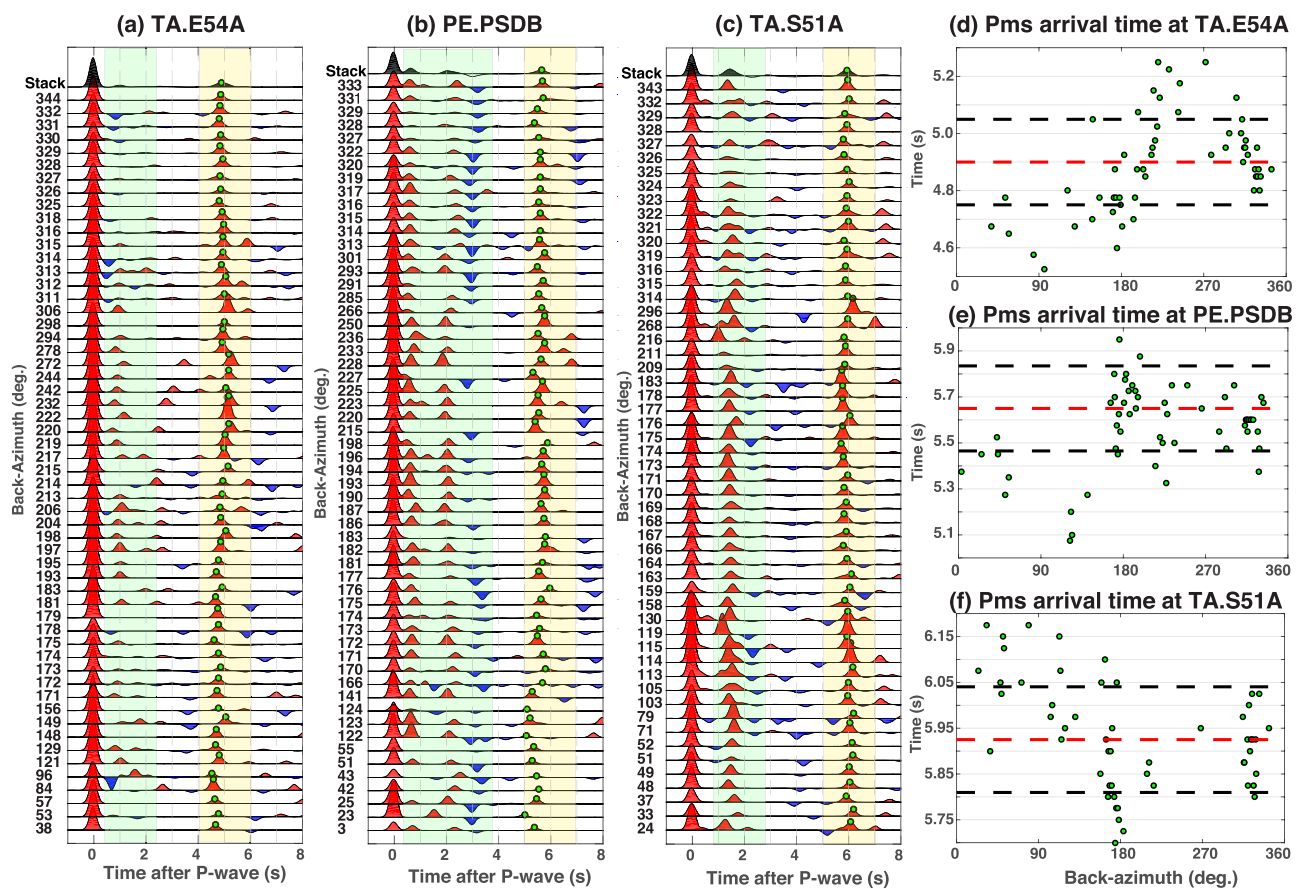


Figure 2. (a–c) Examples of normalized radial-component receiver functions (RF) for stations TA.E54A, PE.PSDB, and TA.S51A, sorted by back azimuths. See station locations in Figure 3. A positive phase (filled with red color) corresponds to a sharp velocity increase with depth, while a negative phase (filled with blue color) correlates with a velocity decrease. The top trace is the stacked receiver function from all the back azimuth directions at each station. The waveforms are low-pass filtered at 2.4 Hz. The green dots mark the automatically picked P_{ms} arrivals. The shaded yellow window highlights the variation pattern of the P_{ms} phase in terms of the back azimuth, and the shaded green window highlights the phases converted from the intracrustal layers. (d–f) Distribution of automatically picked P_{ms} arrival time (green dots) in terms of the back azimuth for the three stations in (a)–(c). The red and black dashed lines correspond to the P_{ms} arrival time of the stacked radial-component receiver functions and the corresponding uncertainty.

requested to have an epicentral distance of 30–95° to each seismic station and the body wave magnitude equal to or greater than 5.5. Supporting information Figure S1 shows the distribution of selected earthquakes, which result in a total of 306,942 waveforms obtained for the RF calculations.

3.2. P Wave Receiver Functions

Prior to the calculation of receiver functions, we cut the raw seismograms to 90 s segments, that is, 30 s before and 60 s after the direct P wave arrival calculated using the one-dimensional velocity model IASP91 (Kennett & Engdahl, 1991). We removed the mean value and the first-order linear trend from the waveforms. The horizontal components were then rotated along the free surface to obtain the radial and transverse components. We calculated teleseismic P wave RFs using the generalized iterative deconvolution method (Wang & Pavlis, 2016). This method significantly improved the resolution of RFs by applying an inverse wavelet on the time domain iterative deconvolution, which can be described in three steps.

First, an inverse wavelet of the source is calculated in the frequency domain as

$$S(\omega) = \frac{Z^*(\omega)}{Z(\omega)Z^*(\omega) + \mu} \quad (1)$$

where $Z(\omega)$ and $Z^*(\omega)$ represent the Fourier transforms of the vertical-component seismogram and its

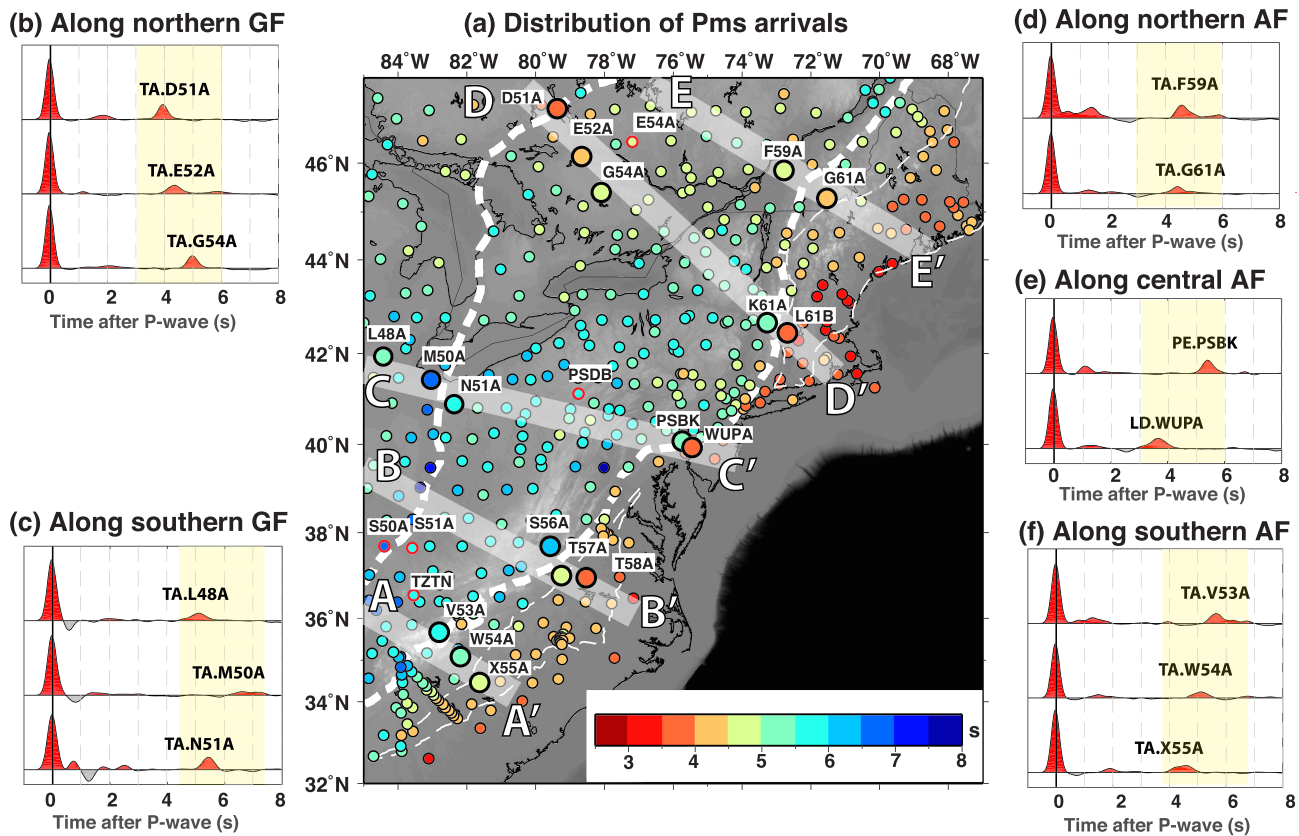


Figure 3. (a) Distribution of P_{mS} arrival time (in seconds), automatically picked from the stacked radial-component receiver functions for each seismic station. Warm colors denote relatively smaller P_{mS} arrivals, and cold colors denote larger P_{mS} arrivals. The five shaded zones are the profile locations shown in Figure 6. The larger dots mark the locations of selected seismic stations in (b)–(f), which are also shown as green dots in Figure 6. The dots with red outline are stations shown in Figures 2 and S16. The thick white dashed lines mark the North American craton-Grenville boundary and the Grenville-Appalachian boundary, respectively. (b–f) Representative radial-component RFs to demonstrate variations of P_{mS} arrival times in eastern North America. For each station, the RFs are stacked from all the back azimuthal directions. The waveforms are low-pass filtered at 2.4 Hz. The shaded yellow window highlights the difference in the P_{mS} arrival times.

complex conjugate, respectively. μ is the background noise level, defined as the standard deviation of the waveforms within a time window of 1–11 s prior to the direct P arrival. Second, we cross-correlate the inverse wavelet with the radial-component seismogram in the time domain. The arrival time and amplitude of the peak spike in cross correlation is then used to define a spike sequence. Third, the residual between the radial-component waveform and the spike sequence is used to replace the original radial-component waveform. Steps 2 and 3 are iteratively repeated until the residual reaches a minimum value of 0.01 and the final spike sequence is the calculated radial-component RF. We then applied a low-pass Gaussian filter of 2.4 Hz on the calculated RFs.

In order to identify plausible phases converted from the Moho (P_{mS}) and other primary intracrustal interfaces, we implemented multiple steps to control the quality of the radial-component RFs. The rule of thumb is that the P_{mS} phase is anticipated as a first-order positive phase, which was taken as our target phase during selection. We first applied a time moveout correction, with an averaged slowness of 0.058 s/km based on the IASP91 model (Park & Levin, 2016), to remove the impact of incident angle on the P_{mS} phase. After time moveout, we visually inspected all observed RFs and manually selected those with a clear positive phase within a time window of 2–8 s. For each station, we then visually reviewed the selected RFs and insured the consistency of the P_{mS} phase within similar back azimuthal directions. Furthermore, the selected RFs were filtered within multiple frequency bands, ranging from 0.05–0.75 and 0.1–1.2 to 0.2–2.0 Hz, to check the stability of the P_{mS} phase.

Previous studies by Ammon (1991) and Cassidy (1992) showed that the amplitude ratio of the radial- and vertical-component RFs preserves information on the velocity contrast across sharp boundaries. Therefore, we normalized the radial-component RFs in terms of the maximum amplitude of the corresponding vertical-component RFs. After normalization, we stacked the RFs from all the back azimuthal directions to represent the average RF feature beneath each station. Stacking highlights the primary phases and increases the signal-to-noise ratio. The time of the maximum positive peak of the stacked RF within a time window of 2–8 s was then automatically picked as the mean P_{ms} arrival time, with the uncertainty calculated as the standard error of the P_{ms} arrival times of all individual events at each station (Figure 2).

Here we chose three stations, TA.E54A, TA.S51A, and PE.PSDB (see the station locations in Figure 3), to illustrate the RF quality within our study region (Figure 2). The two EarthScope Transportable Array stations E54A and S51A have 2 year seismic recordings from 2012 to 2014, and the Penn state network station PSDB has been operating since 2010. We took the average of the RF events coming from the same back azimuthal direction (within 1°) at each station. As demonstrated in Figure 2, a clear P_{ms} conversion is identified within a time window of 4.5–6.2 s after the direct P arrival at all these three stations. The P_{ms} arrival time also shows a certain degree of back azimuthal dependence, which could be related to a dipping Moho or a combination of dipping and anisotropy (Levin & Park, 1997). A further study combining both radial- and transverse-component RFs may help identify possible sources for the directional dependence, but this falls beyond the scope of this study. In addition to the primary P_{ms} conversions at the Moho, strong and consistent signals are observed within the crust at many seismic stations (Figures 2, S14, S15, and S16). For example, station PE.PSDB reveals two positive phases at ~0.5 and ~2.1 s, respectively, and a strong negative phase within a time window of 2.9–3.5 s (Figure 2b). Station TA.S51A demonstrates a clear positive signal at approximately 1.6 s from all the back azimuthal directions (Figure 2c).

The number of selected RF events varies within a broad range among the seismic stations, depending on the operating duration and station location. Most long-running stations recorded high-quality RFs with the event numbers ranging from 40 up to 336 (Figure S2 and Table S1). A few stations, such as PE.PASH and PO.BELQ, have less than 1 year recording periods, which leads to fewer events. The number of RFs for the temporary stations varies within a range of 13–100 (Figure S2 and Table S1). We found that 77 stations show strong crustal reverberations (see station locations in Figure S3 and RF examples in Figure S4), most of which are located within the Atlantic coastal plain. In contrast, we saw clear P_{ms} phases for stations located within the Appalachian basin where thick sediments exist (e.g., Laske et al., 2013), even though multiple positive and negative phases are observed prior to the P_{ms} arrivals (Figures 2b and S15). The different features of RFs observed between stations located within the Appalachian basin and the coastal basin may reflect the different velocity contrasts at the sediment-bedrock interface (Figure S11). The nature of the crustal reverberations in RFs deserves a careful analysis and will be the subject of a follow-up study. In this study, we excluded the stations that have strong reverberations from further analysis considering that the reverberations can interfere with and mask major phases in RFs. In total, we selected 39,237 RFs for 487 broadband stations (~73% of the initially collected stations) to be used for further analysis.

3.3. Migration

We converted the normalized radial-component RFs from all the back azimuthal directions at all the selected stations from the time domain to the depth domain, using the common conversion point (CCP) stacking method (Hansen & Dueker, 2009). Assuming a flat-layer model, the arrival time of the converted P_s phase at a given depth of z is described as

$$T_{Ps}(z) = \int_z^0 \left[\sqrt{Vs(z)^{-2} - P^2} - \sqrt{Vp(z)^{-2} - P^2} \right] dz \quad (2)$$

In this equation, P is the ray parameter, and Vp and Vs are the P and S wave velocities, respectively. Considering the distribution density of seismic stations, we meshed our study area with a horizontal bin size of 20 km and a vertical interval dz of 1 km from the surface down to 150 km depth. We interpolated the three-dimensional shear wave velocity model of the United States by Shen and Ritzwoller (2016) to obtain the seismic velocities beneath each grid point assuming a constant Vp/Vs ratio of 1.78.

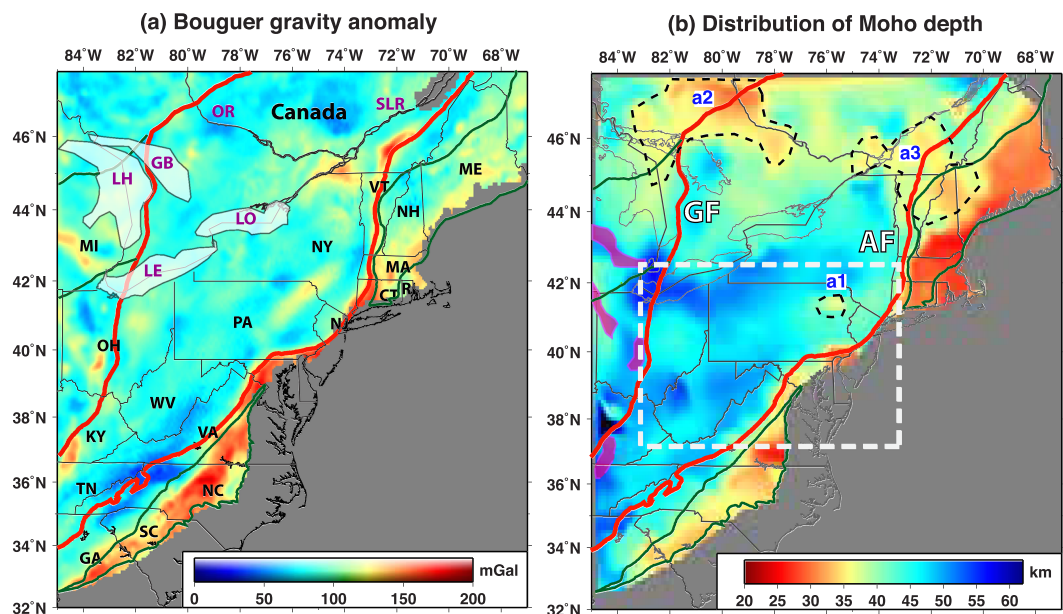


Figure 4. (a) Distribution of Bouguer gravity anomalies from Bonvalot et al. (2012). The red and dark green lines mark the tectonic boundaries as in Figure 1a. (b) Distribution of the Moho depth (in kilometers) extracted from the common conversion point stacking. LO = Lake Ontario; LE = Lake Erie; LH = Lake Huron; GB = Georgian Bay; OR = the Ottawa River; SLR = the St. Lawrence River. The white dashed line marks the map region in Figure 5 where we observe an intracrustal layer. The red solid lines mark the North America craton-Grenville boundary and the Grenville-Appalachian boundary, respectively. The black dashed lines mark the small-scale anomalies observed in the Moho depth map.

The amplitudes of the individual RFs were then back-projected within each bin. In order to estimate the Moho depth beneath each surface grid point, we take the lateral resolution of the Fresnel zone into consideration, which is depth dependent. Here we used the Fresnel zone formula developed by Pavlis (2011) to estimate the aperture size (that is, the lateral resolution) at each depth interval (Figure S5). For example, the radii of the aperture of the CCP stacking are about 10 and 16 km at depths of 20 and 40 km, respectively (Figures S5 and S6). Correspondingly, the RF amplitude at each bin is defined as the averaged amplitude of back-projected RFs within the depth-dependent aperture radius. We then automatically picked the depth of the maximum amplitude of the averaged RFs within a depth range of 20–70 km as the Moho depth. In addition, the CCP stacking also demonstrates strong negative phases at 5–28 km depths within the central Grenville crust. The depth of the maximum amplitude of these negative phases was also automatically picked for further analysis. See the supporting information for the uncertainty estimate of the Moho depth.

4. Results

We investigated the distribution of average arrival times of primary converted phases from the Moho and within the crust, as well as the corresponding depth variations. We observe distinct variations in P_{mS} arrival times and Moho depth in eastern North America (Figures 3 and 4b) on multiple scales. The high resolution of the Moho data set benefits from the combination of a large number of broadband stations that were active over the last decade. In general, the Grenville Province and the North American craton are characterized by larger P_{mS} arrivals and a thicker crust. The Appalachian regions that are interpreted to be underlain by accreted (exotic) terranes show relatively smaller P_{mS} arrival times (i.e., thinner crust). Local variations in Moho depth are delineated clearly, such as a shallow Moho of ~30–35 km in northeastern Pennsylvania, near the Ottawa River and the St. Lawrence River Plain (a1, a2, and a3 in Figure 4). In addition, we also image a distinct intracrustal feature within the central Grenville Province (Figure 5), which we discuss in section 4.3. In order to demonstrate these seismic features, we present five CCP stacking profiles that are nearly perpendicular to the orogenic strike (see profile locations in Figure 3 and cross sections in Figure 6).

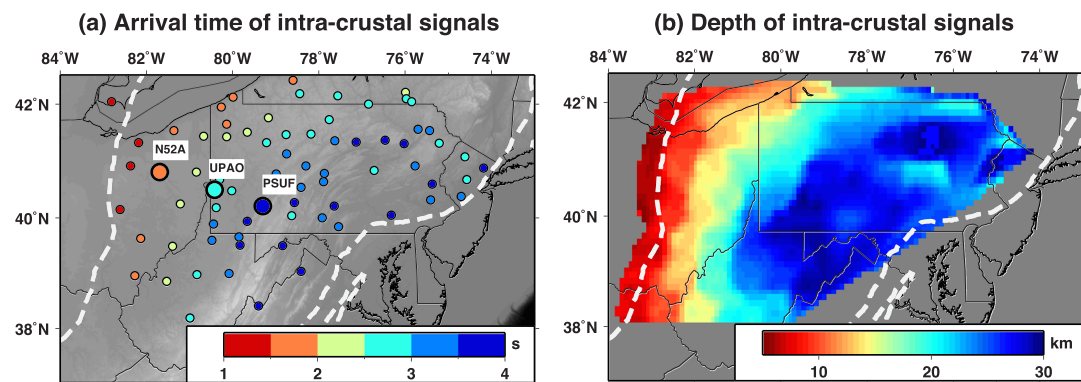


Figure 5. (a) Arrival time distribution of the intracrustal negative phases (in seconds). The three large dots mark the locations of the representative stations in Figure S15. (b) Distribution of the corresponding depth of the intracrustal negative phase, extracted from the common conversion point stacking method.

4.1. Crustal Thickness Variation in the Grenville Province

Grenville-aged crust in eastern North America is characterized by a large variation in P_{ms} arrival time (~4.0–7.0 s) and the associated thickness (~32–65 km). A first-order characteristic is the distinct difference in P_{ms} arrival time (Moho depth) from south to north within the Grenville Province and along the Grenville Front (Figures 3 and 4). The U.S. Grenville Province is characterized by large P_{ms} arrival times (~5.2–7.0 s) and a deep Moho (~47–65 km), extending from Tennessee and Georgia to the national border (Figure 4b). In contrast, the Canadian Grenville Province has P_{ms} arrival times of ~4.0–5.4 s (crustal thickness ~32–50 km).

There is also a significant difference in the P_{ms} arrivals (Moho depth) along and across the Grenville Front. Six seismic stations along the southern Grenville Front show much larger P_{ms} arrivals than the surrounding stations, resulting in a locally deepened Moho (~55–65 km) within a narrow zone from northern Ohio to eastern Kentucky (Figures 3a and 4b and Cross Sections AA', BB', and CC' in Figure 6). For example, a ~7.0 s P_{ms} arrival time (~63 km Moho depth) is seen at station TA.M50A (Figure 3c). In comparison, a relatively smaller P_{ms} arrival of ~5–5.5 s (~46–50 km Moho depth) is imaged at nearby stations TA.L48A and TA.N51A (Figure 3c). Near the northernmost Grenville Front, the small P_{ms} arrivals of ~4–4.5 s and a corresponding shallow Moho of ~32–35 km are detected (see examples in Figure 3b). Note that we do not have resolution in the southernmost and northernmost ends of the Grenville Front near the boundaries of our study area. However, previous studies that investigated the North American craton to west of our study region also show a shallow Moho depth along the northern Grenville Front and support a locally deepened Moho along the southern Grenville Front (Darbyshire et al., 2017; Levin et al., 2017; Petrescu et al., 2016; Yang et al., 2017).

4.2. Moho Depth Variation in the Appalachian Orogen

The Moho depth shows a systematic variation within the Appalachian orogen, ranging from 25 to 45 km. Within the southern Appalachian region, the Moho depth decreases southeastward from ~45 to ~35 km, a 10 km decrease of the Moho depth. Within the northern Appalachian region, the observed Moho depth is ~35–40 km near the Appalachian orogenic Front and decreases southeastward to ~25–30 km toward the coastal plain (Figure 4b).

We observe a significant west-to-east decrease in the Moho depth across the Appalachian orogen. The steepness of the gradient in Moho depth, however, varies significantly along strike (Figures 3a and 4b). A clear and sharp Moho offset of up to 12–15 km is observed within a narrow zone extending from southern New England through New Jersey to Virginia (Figures 3a and 4b). For example, the P_{ms} arrival time (Moho depth) decreases from ~5.4 s (~40 km) to ~3.8 s (~27 km) between stations PE.PSBK and LD.WUPA in New Jersey (Figure 3e and Cross Section CC' in Figure 6). Similarly, between stations TA.K61A and TA.L61B in southern New England, the P_{ms} arrival time decreases from 5.2 to 3.7 s (the corresponding Moho depth changes from ~45 to ~30 km) (see Cross Section DD' in Figures 6, S13a, and S14), over a horizontal distance of ~70 km. Although the actual magnitude of the Moho offset may

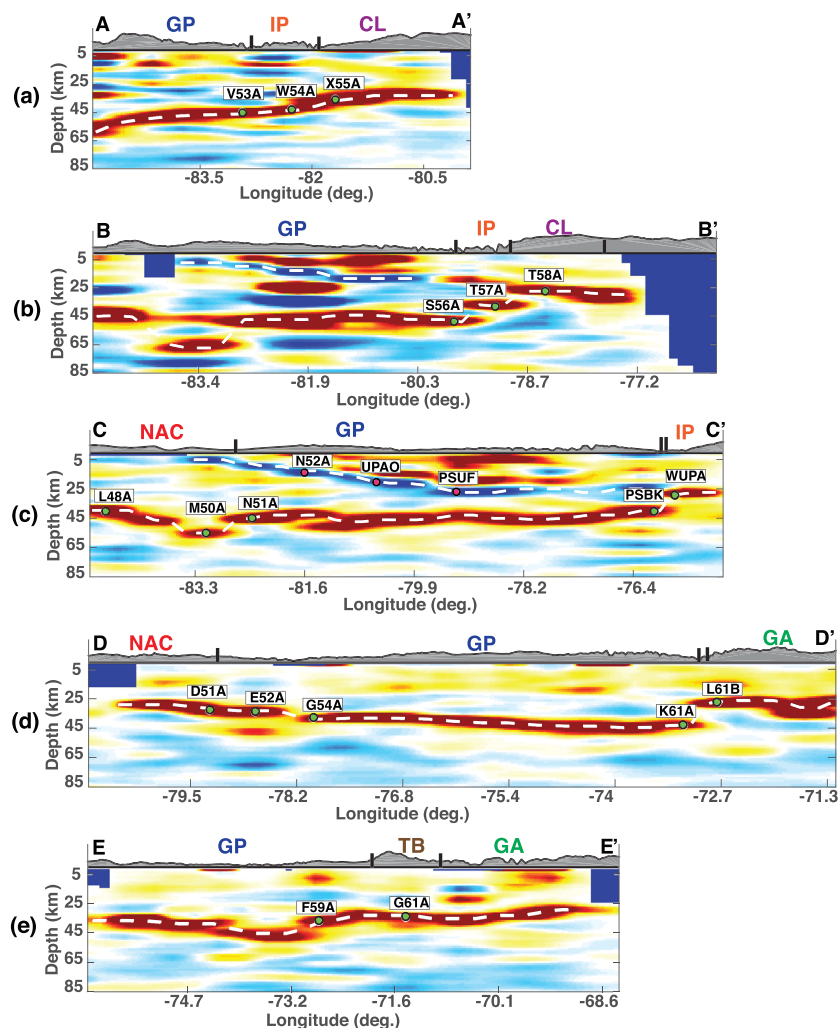


Figure 6. NW-SE cross sections of the common conversion point stacking. See the profile locations in Figure 3. The major tectonic boundaries are marked by solid black lines above each profile. The white dashed line represents the interpreted Moho and intracrustal layer, which are extracted from the common conversion point stacking. The colored dots in the cross section mark the preferred Moho and intracrustal layer beneath seismic stations, as described in the text. IP = Inner Piedmont; CL = Carolina; GA = Gander; GP = Grenville Province; NAC = North American craton.

differ slightly due to the uncertainty of ~6 km in the Moho depth estimation, the uncertainty is much less than the observed Moho offset in our study (see the detailed uncertainty analysis in the supporting information).

In contrast, the Moho depth decreases subtly across the Appalachian orogen in northern New England, southernmost Virginia, western North Carolina, and Georgia. Overall, we image a gradual Moho depth variation across and within the widened northern (north of latitude 45.5°N) and southern (south of latitude 37°N) Appalachian regions. We choose RF results from eight stations (Figures 3d, S13b, and 3f) along Cross Sections AA', BB', and EE' to illustrate the observations. For example, from station TA.V53A to TA.W54A to TA.X55A, we observe a decrease of the P_{mS} arrival time by ~0.7 s across the Grenville-Appalachian boundary and by ~0.5 s across the Piedmont-Carolina boundary (Figure 3f). The corresponding the Moho depth gradually decreases from 50 to 42 to 35 km over a horizontal distance of 190 km (Cross Section AA' in Figure 6). Similarly, a gradual change of P_{mS} arrival and Moho depth is seen from TA.F59A to TA.G61A over ~130 km in the northern Appalachian region (Figure 3d and Cross Section EE' in Figure 6).

4.3. An Eastward Dipping Feature Within the U.S. Grenville Crust

Seismic stations located in the central (from north to south) Grenville Province exhibit a pronounced negative phase within the crust. The phase arrival time gradually increases from the Grenville Front to the east over a horizontal distance of ~700 km, showing an eastward dipping intracrustal feature (Figure 5). As demonstrated in Figure S15, the arrival time of the negative phase gradually increases from station TA.N52A (~1.8 s) to PE.UPAO (~3.0 s) and PE.PSUF (~3.8 s), with the corresponding depths of approximately 10, 20, and 25 km, respectively (Cross Section CC' in Figure 6). Most of the stations that show the negative phase are located in southernmost New York, Pennsylvania, eastern Ohio, and West Virginia (Figure 5). In Kentucky, Tennessee, and Georgia, we are only able to identify a negative phase signal at a few stations (see examples in Figure S16), leading to a less consistent intracrustal layer in our CCP imaging (Cross Sections AA' and BB' in Figure 6). In total, 107 stations, extending from latitude 34°N to 42.5°N, recorded the negative phase signals. Additionally, we see multiple positive phases prior to the negative phase at many stations (see profiles BB' and CC' in Figure 6), which may represent second-order velocity discontinuities within the crust. More specifically, the near-surface positive phase may result from a sedimentary basement (Figure S11), and the later positive and negative phases may represent a high velocity layer or a shear zone with strong seismic anisotropy (Figure S12). However, the nature of these phases, as well as possible interpretations, need to be furthered explored by incorporating data from dense seismic arrays and analyzing the transverse-component receiver functions.

5. Discussion

Our RF results demonstrate a distinct variation in Moho depth both within and across the major tectonic units in eastern North America (Figures 4b and S15). (1) We observe a relatively thick crust (47–65 km) in the United States portion of the Grenville Province and a thinner crust within the Canadian portion (33–50 km). (2) An abrupt Moho deepening (~65 km) can be seen within a narrow zone along the southern part of the geologically defined Grenville Front (Latitude ~37°N to 42.5°N). In contrast, the Moho depth beneath the northernmost Grenville Front is much shallower than beneath the southern part. (3) A strong intracrustal layer is imaged beneath the central Grenville Province, with a low-angle dip of approximately 6° from the Grenville Front eastward to the Appalachian orogen (Figure 5; Cross Section CC' in Figure 6). (4) A sharp west-east Moho step (~12–15 km) is observed over a horizontal distance of ~70 km in the central segment of the Appalachian orogen (from Latitude 37°N to 43.5°N; Cross Sections CC' and DD' in Figure 6). The Moho step tends to be more gradual across the Appalachian Front in the southern and northern segments of Appalachian orogen, where we observe a second-order Moho variation (Cross Sections AA' and EE' in Figure 6). Interestingly, the location of the Moho step diverges from the Appalachian (or Acadian) Front in the northern and southern parts of the Appalachian orogeny, roughly correlated with the widening of the overall orogen (Figure 4b).

The crustal features beneath eastern North America resolved in this study are broadly consistent with the results of previous studies. We specifically compared the distribution patterns of the crustal thickness extracted from this study, Shen and Ritzwoller (2016), and Schmandt et al. (2015) (Figure S18). For example, the general northwestward decrease in crustal thickness from the Grenville Province to the Appalachian region can be seen in several seismological studies (e.g., Gaherty et al., 2011; Li et al., 2002; Li et al., 2018; Schmandt et al., 2015; Shen & Ritzwoller, 2016). The deep Moho beneath the Grenville Province in the United States was also previously recognized even though the horizontal distribution of deep Moho is slightly different between studies (e.g., Schmandt et al., 2015; Shen & Ritzwoller, 2016; Yang et al., 2017). The presence of an intracrustal layer was noted along a 2-D seismic array in Ohio, West Virginia, Georgia, and South Carolina by both receiver function studies (Hopper et al., 2017; Long et al., 2019; Parker et al., 2015) and active source experiments (Culotta et al., 1990; White et al., 2000). Nevertheless, our results provide a comprehensive constraint on both Moho depth variations and the 3-D spatial distribution of the intracrustal layer across the entire eastern North American region, benefiting from the data integration of all broadband stations deployed in this region over the last decade.

5.1. Comparison of Crustal Thickness, Gravity, and Topography

We compared the distribution patterns of crustal thickness, Bouguer gravity, and elevation in eastern North America (Figures 1b and 4). From isostasy theory, we would expect lower Bouguer gravity in the U.S.

Grenville Province, where the crust is thicker than in the Canadian part (Figures 1b and 4). However, we do not observe any systematic variation in Bouguer gravity within the Grenville interior. The lack of correlation between crustal thickness and gravity may reflect a nonuniform density distribution in the crust and upper mantle. It was suggested that the lower crust of the continental lithosphere can be densified and strengthened due to metamorphic reactions (e.g., Fischer, 2002; Williams et al., 2014), which might be expected in the thicker crust of the eastern United States (e.g., Schmandt et al., 2015). A denser lower crust could increase the gravity anomaly of the United States relative to the Canadian portion of the Grenville Province. In addition, geophysical and petrologic studies (e.g., Mooney & Kaban, 2010; Perry et al., 2003) have suggested that the uppermost mantle is less dense and more buoyant in the northern Grenville than in the southern Grenville, which would also help to explain our observations. Some small-scale variations in the Moho depth show (anti)correlation with Bouguer gravity. For example, the locally shallowed Moho in northeastern Pennsylvania roughly corresponds to a relatively large gravity anomaly (a1 in Figure 4b), suggesting a more local isostatic control of Moho depth.

The relationship among crustal thickness, Bouguer gravity, and elevation is also not straightforward within the Appalachian orogen. In the southern Appalachians, for example, we see the expected negative correlation pattern roughly across the Inner Piedmont-Carolina terrane boundary (Hales et al., 1968; James et al., 1968), where the crustal thickness and the elevation show an west-east decrease and a corresponding Bouguer gravity increase (Figures 1b and 4). However, we did not image a Moho depth anomaly beneath the highest southern Appalachian Mountains, where a distinct gravity low exists. The crustal thickness is anticorrelated with the Bouguer gravity along the Appalachian orogen from Latitude $\sim 37^{\circ}\text{N}$ to $\sim 43^{\circ}\text{N}$, where the sharp west-east Moho step is observed. Within the northern Appalachians, the relatively thin crust in the coastal plain roughly corresponds with higher gravity, and a local downward deflection of the Moho is roughly correlated with the low Bouguer gravity anomaly (a3 in Figure 4b). Comparing the northern and southern Appalachians, we observe that the interpreted accreted terranes (Gander and Avalon) in the New England region show a thinner crust with a lower gravity, while the Carolina Superterrane has a relatively thicker crust with a larger gravity anomaly.

5.2. Crustal Thickness Variation Within the Grenville Province

The observed differences in seismic characteristics within the interior of the Grenville Province, especially differences in crustal thickness and the presence of an intracrustal layer, may indicate important differences in the tectonic history from north to south. The reconstruction study by Li et al. (2008) concluded that the U. S. Grenville Province represents a single continent block, which was accreted onto the North American craton at ~ 1.0 Ga. This simple collision mode might have thickened the crust along the southern Grenville Front. In this case, the intracrustal dipping layer in the central Grenville interior could represent the trace of a west-vergent thrust/shear zone that emplaced Grenville-aged crust over the North American craton (Long et al., 2019). In contrast, the Canadian portion of the Grenville Province is interpreted to have formed by a sequence of island arc and microcontinent accretions (e.g., McLelland et al., 2013; Rivers, 2015). Several active source experiments in Canada (e.g., Culotta et al., 1990; Martignole & Calvert, 1996; Rivers, 2015) demonstrated local-scale thrust belts within the northern Grenville crust, supporting the repeated accretion of smaller fragments model. The accretion may have resulted in a more complex network of crustal structures instead of forming a simple intracrustal layer (structure) as observed in the south.

Another possible interpretation for the Grenville crustal variation is that the region may have had a similar prograde history but experienced different degrees of modification during postcollisional collapse and exhumation. Numerical modeling studies by Jamieson et al. (2010) suggested that the northern Grenville experienced strong extensional collapse as the thermally weakened middle and lower crust could no longer support the thick upper crust. In this case, the collapse would eventually result in a thinner crust and might obscure any intracrustal collisional feature in the Canadian Grenville Province. The large-scale erosion during the breakup of Rodinia at ~ 750 Ma might have further thinned the crust. In addition, recent tectonic events, such as the magmatism caused by the Great Meteor hot spot during ~ 140 – 110 Ma (Eaton & Frederiksen, 2007) and a failed rift near the Ottawa River (Rimando & Benn, 2005), also likely modified the Grenville-aged crust in Canada, contributing to the observed south-north differences.

It was recently suggested that the gravity-defined eastern arm of the 1.1-Ga failed Midcontinent Rift extends into Ohio and Kentucky along the southern Grenville Front (cyan patches in Figure 1a; Stein, Stein, Elling,

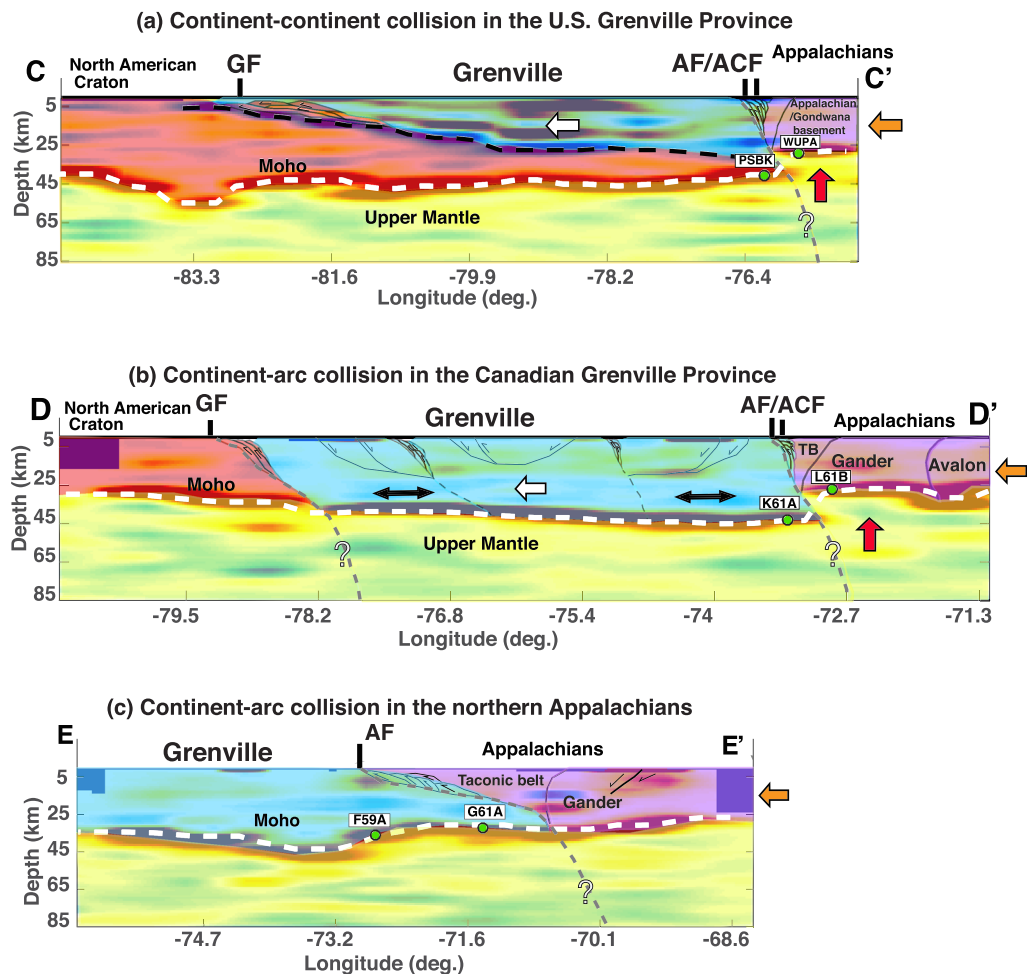


Figure 7. Schematic diagrams illustrating variations of the crustal features and our preferred interpretations along Cross Sections CC', DD', and EE' in eastern North America, modified after McLellan et al. (2010) and Li et al. (2018). (a) Continent-continent collisional model that can be applied to the U.S. Grenville Province. (b) Continent-arc collisional model that can be applied to the Canadian Grenville Province and the central Appalachians. (c) Continent-arc collisional model that can be applied to the northern (and southern) Appalachians. The white dashed lines represent the interpreted Moho, and the black dashed line in (a) reflects an eastward thrusting of the Grenville-aged crust over the North American craton. The gray dotted lines represent our interpreted subsurface extent of the Grenville Front (GF), the Acadian Front (ACF), and the Appalachian Front (AF). The thin black lines with arrows denote the thrust faults during accretion and collision and the normal faults during extensional collapse, according to McLellan et al. (2010). The white arrows in (a) and (b) mark the relative direction of the Grenville Province-North American craton collision during the Grenville orogeny. The orange arrows mark the accretion of a series of terranes onto the Grenville Province. The red arrows represent the uplifting due to the orogenic collapse and rifting. In (b), the black two-headed arrows represent the lateral extensional collapse. The background imaging is from Cross Sections CC', DD' and EE' of our receiver functions, shown in Figure 6.

Keller, & Kley, 2018; Stein, Stein, Elling, Kley, et al., 2018). However, we do not observe any obvious spatial correlation between the eastern arm of the Midcontinent Rift (pink patches in Figure 4b) and the locally deepened Moho imaged by our RF study (Figure 4b). It is likely that the crust was locally thickened during and shortly after the midcontinent rifting due to underplating, sedimentation, and compression (Stein, Stein, Elling, Keller, & Kley, 2018). Compression during the later phases of the Grenville orogeny might have further thickened the crust along the southern Grenville Front, which consequently inverted and overprinted structures associated with the eastern arm of the Midcontinent Rift. After the main collisional pulses, postorogenic erosion would have removed the surface thrust belts along the southern Grenville Front, leaving the local Moho depression as a remnant continental root.

5.3. Moho Depth Variation Within the Appalachian Accretion

The rough correlation of Moho depth with geologically defined terrane boundaries and with Bouguer gravity variation suggests that the large-scale crustal thickness changes in the Appalachian region are linked with the terrane accretion during the assembly of Pangea. Further, **the magnitude and character (dipping or steep) of the Moho offset along the Appalachians may provide additional constraints on tectonic models.** We propose that differences in the steepness of the Moho offset along the Appalachians reflect along-strike variations of the steepness of the subsurface boundary between Laurentian lithosphere and Gondwana-derived elements. Specifically, the gradual Moho depth change beneath the northern and southern Appalachian regions is interpreted to reflect a shallowly dipping Grenville basement beneath the Appalachian accreted terranes. This is supported by the presence of a low-angle southeastward dipping intracrustal layer beneath the Inner Piedmont, Carolina, and northern New England, previously interpreted as a continent-arc collisional interface (e.g., Cook & Vasudevan, 2006; Hopper et al., 2017; Parker et al., 2015; Spencer et al., 1989). In contrast, the sharp Moho step in the central Appalachians may represent a steeply dipping crustal boundary between Laurentian and Gondwana-derived crust (Li et al., 2018).

Our hypothesis that the central segment of the Laurentia-Gondwana boundary dips steeply implies that the central Appalachian crust might have experienced much more significant modification during and after accretion in comparison with the northern and southern parts. For example, Hatcher (2010) suggested that an intensified transpressional collision of the Gander and/or Carolina terranes with the Grenville Province led to a sharp boundary beneath the central Appalachians. Furthermore, the consistency between the location of sharp Moho step and the Acadian deformation front from New England to northern Virginia implies that collisional and possibly transcurrent events may have steepened the subsurface boundary (Cheney & Brady, 1992; Li et al., 2018). In addition, differential uplift caused by a gravitational collapse of the thickened Acadian hinterland could also contribute to steepness of the central boundary. The lack of major tectonic events in eastern North America during the last 200 Ma helps to explain the preservation of a Paleozoic Moho step beneath the central Appalachians.

A steep Moho offset has also been observed in other orogenic settings. For example, a recent *P* wave RF study with a dense seismic array in eastern Tibet found a ~10 km Moho step within a horizontal distance of ~30 km across the boundary between the Songpan-Ganzi block and the Sichuan Basin (Wang et al., 2018). In southernmost New Zealand, a ~12–15 km Moho offset across the boundary between Fiordland and the accreted terranes was suggested by metamorphic mineral analysis (Klepeis et al., 2019). These structural similarities suggest that preserved Moho offsets across tectonic boundaries may be relatively common (or at least not uncommon) across the diversity of collisional environments.

5.4. Possible Crustal Models in Eastern North America

The variation in seismic characteristics may suggest alternative modes of tectonic accretion in the North American Grenville Province. Continent-continent collision can result in a deep Moho and low-angle intracrustal detachments such as in the U.S. Grenville Province (Figure 7a), where the intracrustal interface represents collisional thrusting of the Grenville-aged crust over the North American craton. In this case, the U.S. Grenville Province probably preserves its original Moho. Similar crustal structures have been observed in other orogens, such as the Alleghenian suture in the southeastern United States due to the Laurentia-Gondwana collision (Hopper et al., 2017) and the Himalayan collisional zone due to the collision between Indian and Eurasian continents (Schulte-Pelkum et al., 2005). In contrast, the collision between the North American craton and a series of small tectonic terranes might be more applicable to the Canadian Grenville Province and the Appalachian orogen (Figures 7b and 7c). Repeated accretion and exhumation, as well as later rifting and magmatism, have significantly modified the crust, resulting in a relatively shallow, more heterogeneous Moho and complex intracrustal structure.

6. Conclusions

Teleseismic *P* wave receiver function analysis was used to image the distribution of crustal thickness within eastern North America. Crustal characteristics and Moho depth both vary significantly across and within the major tectonic units. Specifically, a deepened Moho is detected within a narrow zone along the southern part

of the Grenville Front. The U.S. Grenville Province is characterized by a deep Moho and a low-angle eastward dipping intracrustal layer. The northern Grenville crust is relatively thin. Crustal thickness in general decreases from the Grenville Province to the Appalachian orogen, although the magnitude and character of the Moho change varies along strike. A sharp 12–15 km Moho offset is seen in the central Appalachians, and the Moho depth varies more gradually in the north and south. The observed spatial relation between the geologically defined tectonic boundaries and the underlying Moho variations provides new constraints on the depth extent of the tectonic units within the crust.

Acknowledgments

All seismic data were obtained from the IRIS Data Management Center. The depth distributions of the Moho and the intracrustal layer generated in this study will be available through the IRIS Earth Model Collaboration (<https://ds.iris.edu/ds/products/emc-earthmodels/>). The picked P_m s arrivals beneath each station and the CCP stacking data are available at Open Science Framework website (<https://osf.io/j4uqs/>). We acknowledge Yinzhi Wang and Xiaotao Yang for providing codes to calculate the receiver functions and acknowledge Donald U. Wise for the thoughtful discussions about the implications of the receiver function results. We thank the Associate Editor Martha Savage and two anonymous reviewers for their constructive suggestions. This research was supported by the National Science Foundation under Grant EAR-1736167.

References

- Albuquerque Seismological Laboratory (ASL)/USGS (1988). Global seismograph network (GSN - IRIS/USGS). International federation of digital seismograph networks. Dataset/Seismic Network. <https://doi.org/10.7914/SN/IU>
- Albuquerque Seismological Laboratory (ASL)/USGS (1994). New England seismic network. International federation of digital seismograph networks. Dataset/Seismic network. <https://doi.org/10.7914/SN/NE>
- Ammon, C. (1991). The isolation of receiver effects from teleseismic P waveforms. *Bulletin of the Seismological Society of America*, 81(6), 2504–2510. <https://doi.org/10.1029/2005JB004161>
- Bonvalot, S., Balmino, G., Briais, A., Kuhn, M., Peyrefitte, A., Vales, N., et al. (2012). World Gravity Map (scale 1, 50000000. Paris: BGI-CGMW-CNES-IRD.
- Bradley, D. C., Tucker, R. D., Lux, D. R., Harris, A. G., & McGregor, D. C. (2000). Migration of the Acadian Orogen and foreland basin across the northern Appalachians of Maine and adjacent areas. *US Geological Survey Professional Paper*, 1624, 44–50.
- Card, K. D. (1990). A review of the Superior Province of the Canadian shield, a product of Archean accretion. *Precambrian Research*, 48(1–2), 99–156. [https://doi.org/10.1016/0301-9268\(90\)90059-Y](https://doi.org/10.1016/0301-9268(90)90059-Y)
- Cassidy, J. F. (1992). Numerical experiments in broadband receiver function analysis. *Bulletin of the Seismological Society of America*, 82(3), 1453–1474. <http://www.bssaonline.org/content/82/3/1453>
- Cheney, J. T., & Brady, J. B. (1992). Petrology of the high-alumina hoosac schist from the chloritoid+garnet through the kyanite+biotite zones in western Massachusetts. In P. Robinson, & J. B. Brady (Eds.), *Guidebook for field trips in the Connecticut Valley region of Massachusetts and adjacent states*, (pp. 332–357). Amherst, MA: University of Massachusetts, Amherst.
- Colorado Geological Survey (2016). Colorado Geological Survey Seismic Network. International Federation of Digital Seismograph Networks. Dataset/Seismic Network. <https://doi.org/10.7914/SN/C0>
- Cook, F. A., & Vasudevan, K. (2006). Reprocessing and enhanced interpretation of the initial COCORP southern Appalachians traverse. *Tectonophysics*, 420(1–2), 161–174. <https://doi.org/10.1016/j.tecto.2006.01.022>
- Culotta, R. C., Pratt, T., & Oliver, J. (1990). A tale of two sutures: COCORP's deep seismic surveys of the Grenville province in the eastern U.S. midcontinent. *Geology*, 18(7), 646–649. [https://doi.org/10.1130/0091-7613\(1990\)018<0646:ATOTSC>2.3.CO;2](https://doi.org/10.1130/0091-7613(1990)018<0646:ATOTSC>2.3.CO;2)
- Darbyshire, F. A., Bastow, I. D., Petrescu, L., Gilligan, A., & Thompson, D. A. (2017). A tale of two orogens: Crustal processes in the Proterozoic trans-Hudson and Grenville Orogens, eastern Canada. *Tectonics*, 36, 1633–1659. <https://doi.org/10.1002/2017TC004479>
- David, J., Godin, L., Stevenson, R., O'Neil, J., & Francis, D. (2009). U-Pb ages (3.8–2.7 Ga) and Nd isotope data from the newly identified Eoarchean Nuuvuagittuq supracrustal belt, superior Craton, Canada. *Bulletin of the Geological Society of America*, 121(1–2), 150–163. <https://doi.org/10.1130/B26369.1>
- Eaton, D. W., & Frederiksen, A. (2007). Seismic evidence for convection-driven motion of the North American plate. *Nature*, 446(7134), 428–431. <https://doi.org/10.1038/nature05675>
- Fischer, K. M. (2002). Waning buoyancy in the crustal roots of old mountains. *Nature*, 417(6892), 933–936. <https://doi.org/10.1038/nature00855>
- Fischer, K. M., Hawman, R. B., & Wagner L. S., (2010). Southeastern suture of the Appalachian Margin Experiment. International Federation of Digital Seismograph Networks. Dataset/Seismic Network. https://doi.org/10.7914/SN/Z9_2010
- Gaherty, J. B., Dalton, C., & Levin, V. (2011). A three-dimensional model of crustal structure in the central and eastern US derived from broadband ambient-noise surface waves and receiver functions. United States: U.S. Geological Survey.
- Gaherty, J. B., Wagner, L. S., Becel, A., Benoit, M., Long, M. D., Shillington, D., et al. (2014). Eastern North American Margin Community Seismic Experiment. International Federation of Digital Seismograph Networks. Dataset/Seismic Network. https://doi.org/10.7914/SN/YO_2014
- Geological Survey of Canada (1989). Canadian National Seismograph Network. International Federation of Digital Seismograph Networks. Dataset/Seismic Network. <https://doi.org/10.7914/SN/CN>
- Geological Survey of Canada (2000). Portable Observatories for Lithospheric Analysis and Research Investigating Seismicity (POLARIS). International Federation of Digital Seismograph Networks. Dataset/Seismic Network.
- Hales, A. L., Helsley, C. E., Dowling, J. J., & Nation, J. B. (1968). The east coast onshore-offshore experiment, I. The first arrival phases. *Bulletin of the Seismological Society of America*, 58(3), 757–819.
- Hansen, S., & Dueker, K. (2009). P - and S -wave receiver function images of crustal imbrication beneath the Cheyenne belt in southeast Wyoming. *Bulletin of the Seismological Society of America*, 99(3), 1953–1961. <https://doi.org/10.1785/0120080168>
- Hatcher, R. D. (2010). The Appalachian orogen: A brief summary, from Rodinia to Pangea: The lithotectonic record of the Appalachian region. *The Geological Society of America Memoir*, 206, 1–19. [https://doi.org/10.1130/2010.1206\(01](https://doi.org/10.1130/2010.1206(01)
- Hibbard, J. P., & Karabinos, P. (2013). Disparate paths in the geologic evolution of the northern and southern Appalachians: A case for inherited contrasting crustal/lithospheric substrates. *Geoscience Canada*, 40(4), 303–317. <https://doi.org/10.12789/geocanj.2013.40.021>
- Hibbard, J. P., Van Staal, C. R., Rankin, D. W., & Williams, H. (2006). Lithotectonic MAP of the Appalachian orogen (MAP NO. 2096A, scale 1:5000000). Canada–United States of America: Geological Survey of Canada.
- Hopper, E., Fischer, K. M., Wagner, L. S., & Hawman, R. B. (2017). Reconstructing the end of the Appalachian orogeny. *Geology*, 45(1), 15–18. <https://doi.org/10.1130/G38453.1>
- Hynes, A., & Rivers, T. (2010). Protracted continental collision; evidence from the Grenville Orogen. *Canadian Journal of Earth Sciences*, 47(5), 591–620. <https://doi.org/10.1139/E10-003>
- IRIS Transportable Array (2003). USArray Transportable Array: International Federation of Digital Seismograph Networks. Other/Seismic Network. <https://doi.org/10.7914/SN/TA>

- James, D. E., Smith, T. J., & Steinhart, J. S. (1968). Crustal structure of the middle Atlantic states. *Journal of Geophysical Research*, 73(6). <https://doi.org/10.1029/JB073i006p01983>
- Jamieson, R. A., Beaumont, C., Warren, C. J., & Nguyen, M. (2010). The Grenville Orogen explained? Applications and limitations of integrating numerical models with geological and geophysical data. *Canadian Journal of Earth Sciences*, 47, 517–539. <https://doi.org/10.1139/E09-070>
- Karabinos, P., MacDonald, F. A., & Crowley, J. L. (2017). Bridging the gap between the foreland and hinterland I: Geochronology and plate tectonic geometry of Ordovician magmatism and terrane accretion on the Laurentian margin of New England. *American Journal of Science*, 317(5), 515–554. <https://doi.org/10.2475/05.2017.01>
- Kennett, B. L. N., & Engdahl, E. R. (1991). Traveltimes for global earthquake location and phase identification. *Geophysical Journal International*, 105(2), 429–465. <https://doi.org/10.1111/j.1365-246X.1991.tb06724.x>
- Kentucky Geological Survey/Univ. of Kentucky (1982). Kentucky Seismic and Strong Motion Network. University of Kentucky. Dataset/Seismic Network. <https://doi.org/10.7914/SN/KY>
- Klepeis, K., Webb, L., Blatchford, H., Schwartz, J., Jongens, R., Turnbull, R., & Stowell, H. (2019). Deep slab collision during Miocene subduction causes uplift along crustal-scale reverse faults in Fiordland, New Zealand. *GSA Today*, 29(9). <https://doi.org/10.1130/GSATG399A.1>
- Lamont Doherty Earth Observatory (LDEO), Columbia University (1970). Lamont-Doherty Cooperative Seismographic Network (LCSN). International Federation of Digital Seismograph Networks. Dataset/Seismic Network.
- Laske, G., Masters, G., Ma, Z., & Pasyanos, M. (2013). Update on CRUST1.0—A 1-degree global model of Earth's crust. *Geophysical Research Abstracts*, 15.
- Levin, V., & Park, J. (1997). P-SH conversions in a flat-layered medium with anisotropy of arbitrary orientation. *Geophysical Journal International*, 131(2), 253–266. <https://doi.org/10.1111/j.1365-246X.1997.tb01220.x>
- Levin, V., Servali, A., Van Tongeren, J., Menke, W., & Darbyshire, F. (2017). Crust-mantle boundary in eastern North America, from the (oldest) craton to the (youngest) rift: The crust-mantle and lithosphere-asthenosphere boundaries: Insights from xenoliths, orogenic deep sections and geophysical studies. In G. Bianchini, et al. (Eds.), *The Geological Society of America special paper*, (Vol. 526, pp. 107–131). Denver, Colorado: Geological Society of America. [https://doi.org/10.1130/2017.2526\(06\)](https://doi.org/10.1130/2017.2526(06))
- Li, A., Fischer, K. M., van der Lee, S., & Wysession, M. E. (2002). Crust and upper mantle discontinuity structure beneath eastern North America. *Journal of Geophysical Research*, 107(B5), 2100. <https://doi.org/10.1029/2001JB000190>
- Li, C., Gao, H., Williams, M. L., & Levin, V. (2018). Crustal thickness variation in the northern Appalachian Mountains: Implications for the geometry of 3-D tectonic boundaries within the crust. *Geophysical Research Letters*, 45, 6061–6070. <https://doi.org/10.1029/2018GL078777>
- Li, Z. X., Bogdanova, S. V., Collins, A. S., Davidson, A., de Waele, B., Ernst, R. E., et al. (2008). Assembly, configuration, and break-up history of Rodinia: A synthesis. *Precambrian Research*, 160(1–2), 179–210. <https://doi.org/10.1016/j.precamres.2007.04.021>
- Loewy, S. L., Connelly, J. N., Dalziel, I. W. D., & Gower, C. F. (2003). Eastern Laurentia in Rodinia: Constraints from whole-rock Pb and U/Pb geochronology. *Tectonophysics*, 375, 169–197. [https://doi.org/10.1016/S0040-1951\(03\)00338-X](https://doi.org/10.1016/S0040-1951(03)00338-X)
- Long, M. D., Benoit, M. H., Aragon, J. C., & King, S. D. (2019). Seismic imaging of mid-crustal structure beneath central and eastern North America: Possibly the elusive Grenville deformation? *Geology*, 47(4), 371–374. <https://doi.org/10.1130/G46077.1>
- Martignole, J., & Calvert, A. J. (1996). Crustal-scale shortening and extension across the Grenville Province of western Québec. *Tectonics*, 15(2), 376–386. <https://doi.org/10.1029/95TC03748>
- McLellan, J. M., Selleck, B. W., & Bickford, M. E. (2010). Review of the Proterozoic evolution of the Grenville Province, its Adirondack outlier, and the Mesoproterozoic inliers of the Appalachians. *The Geological Society of America Memoir*, 206(02), 21–49. [https://doi.org/10.1130/2010.1206\(02\)](https://doi.org/10.1130/2010.1206(02))
- McLellan, J. M., Selleck, B. W., & Bickford, M. E. (2013). Tectonic evolution of the Adirondack Mountains and Grenville Orogen inliers within the USA. *Geoscience Canada*, 40(4), 318. <https://doi.org/10.12789/geocanj.2013.40.022>
- Meltzer, A. (2011). RAMP Virginia. International Federation of Digital Seismograph Networks. Dataset/Seismic Network. https://doi.org/10.7914/SN/YC_2011
- Menke, W., Levin, V., & Darbyshire, F. (2012). Deep structure of three continental sutures in eastern North America. International Federation of Digital Seismograph Networks. Dataset/Seismic Network. https://doi.org/10.7914/SN/X8_2012
- Mooney, W. D., & Kaban, M. K. (2010). The North American upper mantle: Density, composition, and evolution. *Journal of Geophysical Research*, 115, B12424. <https://doi.org/10.1029/2010JB000866>
- Mount, V. S. (2014). Structural style of the Appalachian Plateau fold belt, north-central Pennsylvania. *Journal of Structural Geology*, 69, 284–303. <https://doi.org/10.1016/j.jsg.2014.04.005>
- Park, J., & Levin, V. (2016). Statistics and frequency-domain moveout for multiple-taper receiver functions. *Geophysical Journal International*, 207(1), 512–527. <https://doi.org/10.1093/gji/ggw291>
- Parker, H. E., Hawman, R. B., Fischer, K. M., & Wagner, L. S. (2015). Constraining lithologic variability along the Alleghanian detachment in the southern Appalachians using passive-source seismology. *Geology*, 43(5), 431–434. <https://doi.org/10.1130/G36517.1>
- Pavlis, G. L. (2011). Three-dimensional, wavefield imaging of broadband seismic array data. *Computers and Geosciences*, 37(8), 1054–1066. <https://doi.org/10.1016/j.cageo.2010.11.015>
- Penn State University (2004). Pennsylvania State Seismic Network. International Federation of Digital Seismograph Networks. Dataset/Seismic Network. <https://doi.org/10.7914/SN/PE>
- Penn State University (2013). PASEIS Network. International Federation of Digital Seismograph Networks. Dataset/Seismic Network.
- Percival, J. A., Bleeker, W., Cook, F. A., Rivers, T., Ross, G., & van Staal, C. (2004). PanLITHOPROBE workshop IV: Intra-orogen correlations and comparative orogenic anatomy. *Geoscience Canada*, 31(1), 23–39.
- Perry, H. K. C., Forte, A. M., & Eaton, D. W. S. (2003). Upper-mantle thermochemical structure below North America from seismic-geodynamic flow models. *Geophysical Journal International*, 154(2), 279–299. <https://doi.org/10.1046/j.1365-246X.2003.01961.x>
- Petrescu, L., Bastow, I. D., Darbyshire, F. A., Gilligan, A., Bodin, T., Menke, W., & Levin, V. (2016). Three billion years of crustal evolution in eastern Canada: Constraints from receiver functions. *Journal of Geophysical Research: Solid Earth*, 121, 788–811. <https://doi.org/10.1002/2015JB012348>
- Rimando, R. E., & Benn, K. (2005). Evolution of faulting and paleo-stress field within the Ottawa graben, Canada. *Journal of Geodynamics*, 39(4), 337–360. <https://doi.org/10.1016/j.jog.2005.01.003>
- Rivers, T. (1997). Lithotectonic elements of the Grenville Province: Review and tectonic implications. *Precambrian Research*, 86(3–4), 117–154. [https://doi.org/10.1016/S0301-9268\(97\)00038-7](https://doi.org/10.1016/S0301-9268(97)00038-7)

- Rivers, T. (2015). Tectonic setting and evolution of the Grenville Orogen: An assessment of progress over the last 40 years. *Geoscience Canada*, 42(1), 77–124. <https://doi.org/10.12789/geocanj.2014.41.057>
- Robinson, P., Tucker, R. D., Bradley, D., Berry, H. N., & Osberg, P. H. (1998). Paleozoic orogens in New England, USA. *GFF*, 120(2), 119–148. <https://doi.org/10.1080/11035899801202119>
- Schmandt, B., Lin, F. C., & Karlstrom, K. E. (2015). Distinct crustal isostasy trends east and west of the Rocky Mountain front. *Geophysical Research Letters*, 42, 290–10,298. <https://doi.org/10.1002/2015GL066593>
- Schulte-Pelkum, V., Monsalve, G., Sheehan, A., Pandey, M. R., Sapkota, S., Bilham, R., & Wu, F. (2005). Imaging the Indian subcontinent beneath the Himalaya. *Nature*, 435(7046), 1222–1225. <https://doi.org/10.1038/nature03678>
- Shen, W., & Ritzwoller, M. H. (2016). Crustal and uppermost mantle structure beneath the United States. *Journal of Geophysical Research: Solid Earth*, 121, 4306–4342. <https://doi.org/10.1002/2016JB012887>
- Soto-Cordero, L., Meltzer, A., & Stachnik, J. C. (2018). Crustal structure, intraplate seismicity, and seismic hazard in the mid-Atlantic United States. *Seismological Research Letters*, 89(1), 241–252. <https://doi.org/10.1785/0220170084>
- Spencer, C., Green, A., Morel-à-l'Huissier, P., Milkereit, B., Luetgert, J., Stewart, D., et al. (1989). The extension of Grenville basement beneath the northern Appalachians: Results from the Quebec-Maine seismic reflection and refraction surveys. *Tectonics*, 8(4), 677–696. <https://doi.org/10.1029/TC008i004p00677>
- Stein, C. A., Stein, S., Elling, R., Keller, G. R., & Kley, J. (2018). Is the “Grenville Front” in the central United States really the Midcontinent Rift? *GSA Today (Geological Society of America)*, 28(5), 4–10. <https://doi.org/10.1130/GSATG357A.1>
- Stein, S., Stein, C. A., Elling, R., Kley, J., Keller, G. R., Wyssession, M., et al. (2018). Insights from North America’s failed Midcontinent Rift into the evolution of continental rifts and passive continental margins. *Tectonophysics*, 744, 403–421. <https://doi.org/10.1016/j.tecto.2018.07.021>
- Thomas, W. A. (2006). Tectonic inheritance at a continental margin. *GSA Today*, 16(2), 4–11. [https://doi.org/10.1130/1052-5173\(2006\)016\[4:TIAACM\]2.0.CO;2](https://doi.org/10.1130/1052-5173(2006)016[4:TIAACM]2.0.CO;2)
- UC San Diego (2013). Central and Eastern US Network. International Federation of Digital Seismograph Networks. Other/Seismic Network. <https://doi.org/10.7914/SN/N4>
- University of Memphis (1982). CERI Southern Appalachian Seismic Network. International Federation of Digital Seismograph Networks. Dataset/Seismic Network.
- University of Western Ontario (1991). The Southern Ontario Seismic Network. International Federation of Digital Seismograph Networks. Dataset/Seismic Network.
- van Staal, C. R., Whalen, J. B., Valverde-Vaquero, P., Zagorevski, A., & Rogers, N. (2009). Pre-carboniferous, episodic accretion-related, orogenesis along the Laurentian margin of the northern Appalachians. *Geological Society, London, Special Publications*, 327(1), 271–316. <https://doi.org/10.1144/SP327.13>
- Wagner, L. (2009). Appalachian seismic transect. International Federation of Digital Seismograph Networks. Dataset/Seismic Network. https://doi.org/10.7914/SN/Z4_2009
- Wagner, L. (2012). Pre-hydrofracking regional assessment of central Carolina seismicity. International Federation of Digital Seismograph Networks. Dataset/Seismic Network. https://doi.org/10.7914/SN/XQ_2012
- Wang, X., Chen, L., Ai, Y., Xu, T., Jiang, M., Ling, Y., & Gao, Y. (2018). Crustal structure and deformation beneath eastern and northeastern Tibet revealed by P-wave receiver functions. *Earth and Planetary Science Letters*, 497, 69–79. <https://doi.org/10.1016/j.epsl.2018.06.007>
- Wang, Y., & Pavlis, G. L. (2016). Generalized iterative deconvolution for receiver function estimation. *Geophysical Journal International*, 204(2), 1086–1099. <https://doi.org/10.1093/gji/ggv503>
- White, D. J., Forsyth, D. A., Asudeh, I., Carr, S. D., Wu, H., Easton, R. M., & Mereu, R. F. (2000). A seismic-based cross-section of the Grenville Orogen in southern Ontario and western Quebec. *Canadian Journal of Earth Sciences*, 37(2–3), 183–192. <https://doi.org/10.1139/CJES-37-2-3-183>
- Whitmeyer, S., & Karlstrom, K. E. (2007). Tectonic model for the Proterozoic growth of North America. *Geosphere*, 3(4), 220–259. <https://doi.org/10.1130/GES00055.1>
- Williams, M. L., Dumond, G., Mahan, K., Regan, S., & Holland, M. (2014). Garnet-forming reactions in felsic orthogneiss: Implications for densification and strengthening of the lower continental crust. *Earth and Planetary Science Letters*, 405, 207–219. <https://doi.org/10.1016/j.epsl.2014.08.030>
- Yang, X., Pavlis, G. L., Hamburger, M. W., Marshak, S., Gilbert, H., Rupp, J., et al. (2017). Detailed crustal thickness variations beneath the Illinois Basin area: Implications for crustal evolution of the midcontinent. *Journal of Geophysical Research: Solid Earth*, 122, 6323–6345. <https://doi.org/10.1002/2017JB014150>